Volume 163, issues 1–4, 1 June 2007
Completing volume 163
ISSN 0377–0273

Available online at www.sciencedirect.com
ScienceDirect
Journal of Volcanology and Geothermal Research 163 (2007) 83–97
Journal of volcanology and geothermal research
www.elsevier.com/locate/jvolgeores

Explosive volcanic eruptions on Mars: Tephra and accretionary lapilli formation, dispersal and recognition in the geologic record

Lionel Wilson [a,1], James W. Head [b,*]

[a] Environmental Science Department, Lancaster University Lancaster LA1 4YQ, UK
[b] Department of Geological Sciences, Brown University, Providence, RI 02912, USA

Received 1 November 2006; received in revised form 7 March 2007; accepted 24 March 2007
Available online 31 March 2007

Abstract

Explosive volcanic eruptions, potentially involving large amounts of magmatic and entrained water, are thought to have been very important in the Noachian and Hesperian periods earlier in Mars history, and basaltic plinian eruptions are likely to have occurred throughout martian history. Previous treatments of explosive volcanic plumes on Mars have simply extrapolated plume models for the Earth's atmosphere to Mars. Taking account of known limitations to the applicability of this approach, which suggest that convective plumes may be capable of reaching only ~20 km height on Mars, we introduce the concept of inertial plumes, capable of carrying clasts to much greater heights and dropping them into the lower atmosphere over a wide area. Atmospheric circulation patterns guarantee wide dispersal and thick deposits of tephra resulting from both types of eruption. The presence of large amounts of water in convecting explosive eruption plumes can also lead to condensation of water on small particles and the consequent accretion of other particles as the smaller particles fall through the plume, producing accretionary lapilli. Formation of accretionary lapilli significantly alters the spatial distribution and grain sizes of pyroclastic fall deposits from those involving discrete juvenile clasts with negligible clast interactions. We model the eruption and dispersal of tephra, and the formation of accretionary lapilli on Mars under current atmospheric conditions and explore the consequences of this for the geometry and grain size of deposits formed from explosive eruption plumes. We show that explosive eruptions can produce thick widespread deposits of ash and lapilli similar to those thought to have produced mantling deposits in several regions of Mars. We develop a detailed example that shows that local hydrovolcanic explosive eruptions and solely magmatic eruptions originating from the nearby Apollinaris Patera could have emplaced tephra and accretionary lapilli in the Columbia Hills region of the Mars Exploration Rover Gusev site. If the atmospheric pressure was higher early in Mars' history than now, eruptions would have led to somewhat more extensive pyroclast dispersal than under current conditions.

Keywords: Mars; explosive eruptions; tephra; lapilli; volcanoes

1. Introduction

Volcanism has been an important process on Mars throughout its history, generally decreasing in significance as a function of time (Tanaka et al., 1992). During the last half of the history of Mars, volcanic activity has been largely centered on the Tharsis and Elysium

* Corresponding author. Tel.: +1 401 863 3526; fax: +1 401 863 3978.
E-mail addresses: l.wilson@lancaster.ac.uk (L. Wilson), james_head@brown.edu (J.W. Head).
[1] Tel.: +44 1524 593889; fax: +44 1524 593985.

0377-0273/$ - see front matter © 2007 Elsevier B.V. All rights reserved.
doi:10.1016/j.jvolgeores.2007.03.007

regions, producing huge shield volcanoes and their associated extensive aprons of lava flows and potential basaltic plinian eruptions (e.g., Wilson and Head, 1994). Earlier in the history of Mars, some of the large volcanic edifices known as paterae (e.g., Hadriaca and Tyrrhena Paterae) were characterized by low constructs and large central craters, strongly suggesting that eruption styles were different in this early period (Greeley et al., 2000). Large expanses of fine-grained deposits mantling subjacent cratered terrain also characterized this period (e.g., Grant and Schultz, 1990; Moore, 1990; Fassett and Head, in press), and these distinctive attributes led many to interpret these early edifices and deposits as being related to specific styles of explosive volcanism that appeared to be dominant during this time, in contrast to the largely effusive nature of the later shield-building eruptions (Carr, 1973; Greeley and Spudis, 1981; Greeley et al., 2000). Higher volatile contents and/or the incorporation of groundwater into the eruptions were thought to be the major causes of the early distinctive explosive eruption style (e.g., Greeley and Crown, 1990; Crown and Greeley, 1993; Robinson et al., 1993). Numerous investigators have developed models for explosive eruptions on Mars and the emplacement of airfall and pyroclastic flow deposits (e.g., see Wilson and Head, 1994, and references therein; Kieffer, 1995; Hort and Weitz, 2001; Glaze and Baloga, 2002) and others have discussed the relationship of models and specific deposits on Mars (e.g., Hynek et al., 2003).

Early application to Mars of eruption plume models developed for the Earth suggested that such plumes should rise much higher in the atmosphere of Mars for a given mass eruption rate (Wilson and Head, 1994). However, Glaze and Baloga (2002) pointed out that some of the assumptions made in these models about the mechanism of entrainment of atmospheric gases are not justified above ~20 km in the atmosphere of Mars, so that high discharge-rate eruptions generating plumes that might have been expected to convect to much greater heights will not behave entirely as predicted. Although we recognize the uncertainties and incomplete aspects of modelling convective plumes in variable atmospheres, we will use this value of 20 km as a limiting value; we infer that, for sufficiently high magma mass fluxes and eruption speeds, explosive eruptions on Mars may instead produce structures more analogous to the umbrella-shaped plumes on Io (Cook et al., 1979; Glaze and Baloga, 2000; Cataldo et al., 2002; Geissler, 2003; Zhang et al., 2003), where gas–particle interactions are minimal except near the surface. We therefore model separately the dispersal of pyroclasts on Mars from convective *plumes* rising to heights up to ~20 km, and *inertial plumes* rising to greater heights.

Furthermore, most treatments of the formation of fall deposits from volcanic eruption plumes on Mars (e.g., Mouginis-Mark et al., 1982, 1988; Kusanagi and Matsui, 1998; Hort and Weitz, 2001) have assumed that individual clasts were transported through, and fell from, such plumes as discrete objects with negligible mutual interactions. However, it is well established that the formation of accretionary lapilli, a mechanism that allows small particles to fall much more rapidly as members of clusters than as individuals, is an important factor in determining the spatial thickness and grain size variations in fall deposits on Earth (e.g., Veitch and Woods, 2001 and references therein). We therefore also explore the nature of this process in the martian environment. We begin by exploring factors influencing the nature of all long-lived, relatively steady discharge rate explosive eruptions on Mars under current atmospheric conditions.

2. Physics of steady explosive eruptions on Mars

The nature of an explosive volcanic eruption depends most strongly on the amount of volatiles released from the magma during its ascent, the key threshold being the release of enough volatiles to ensure that the magma is disrupted into a spray of pyroclasts entrained in the liberated gas. Gas expansion as the pressure decreases is the main source of energy causing high eruption speeds. The gas expansion is accommodated by a mixture of the increase in speed of the gas–pyroclast mixture and the widening toward the surface of the conduit or fissure (Wilson and Head, 1981; Mitchell, 2005). It is likely that in the vast majority of eruptions under current martian conditions, the vent cannot flare outward toward the surface sufficiently rapidly to allow the pressure in the erupting jet of volcanic gas and entrained pyroclasts to decrease to the atmospheric pressure (e.g., Glaze and Baloga, 2002; Mitchell, 2005). Instead the eruption is choked, with the pressure in the vent being the value at which the velocity of the gas–pyroclast mixture is equal to the speed of sound in that mixture. The speed of sound, U_s, in the gas–pyroclast mixture is given with sufficient accuracy (Wilson and Head, 1981) by

$$U_s^2 = (n\ Q\ T/m)\{1 + [((1-n)\ m\ P_v)/(n\ Q\ T\rho_m)]\}^2, \quad (1)$$

where n is the exsolved mass fraction of the major volatile in the magma, here assumed to be dominated by water vapor with molecular weight m equal to 18.02 kg/kmol, Q is the universal gas constant, 8314 J kmol^{-1}

K^{-1}, T is the temperature of the eruption products, taken as 1450 K for a mafic magma, ρ_m is the density of the magmatic liquid, taken as 3000 kg m^{-3}, and P_v is the pressure in the choked flow in the vent.

The speed of the erupting mixture is determined by the amount of expansion of the magmatic gas between the level at which the magma disrupts into pyroclasts and the vent. Using the common assumption that little gas exsolution occurs between the fragmentation level and the surface, and that fragmentation takes place when the volume fraction of gas bubbles in the magma exceeds a critical value of order 0.75, we find that the pressure at the fragmentation level is P_f where

$$P_f = [n\ Q\ T\rho_m]/[3\ (1-n)\ m]. \quad (2)$$

The second column of Table 1 shows how P_f varies with n.

Equating the energy obtained from the decompression of the erupting mixture between the pressures P_f and P_v to the kinetic energy of the eruption products gives (Wilson, 1980)

$$U_v^2 = 2\ (n\ Q\ T/m)\ \ln\ (P_f/P_v). \quad (3)$$

The choked condition requires equating U_v to U_s at the vent, so that

$$\{1 + [((1-n)\ m\ P_v)/(n\ Q\ T\rho_m)]\}^2 = 2\ \ln\ (P_f/P_v) + \{[2\ m\ (1-n)\ (P_f - P_v)]/(n\ Q\ T\rho_m)\}. \quad (4)$$

Given any choice of n and hence P_f from Table 1, this equation can be solved recursively by inserting an initial estimate of the value of P_v (one half of P_f is appropriate) into the right-hand side and solving the equation to obtain an improved estimate of P_v. After an adequate level of convergence has been obtained, either of Eqs. (1) or (3) can be used to obtain the mean eruption speed U_v. The third and fourth columns of Table 1 show the results.

Table 1
Parameters involved in the calculation of eruption conditions on Mars and Earth

n (%)	P_f (MPa)	P_v (MPa)	U_v (m s^{-1})	U_{aM} (m s^{-1})	U_{aE} (m s^{-1})
0.1	0.60	0.30	35	95	46
0.3	1.81	0.92	61	176	104
0.5	3.03	1.53	79	234	146
1.0	6.08	3.07	112	340	227
1.5	9.17	4.63	137	421	290
2.0	12.29	6.21	158	488	344
3.5	21.84	11.03	209	642	475
5.0	31.69	16.01	250	756	577

As a function of the exsolved magma water content, n (given as mass %), values are listed for the pressure, P_f, at the level beneath the surface where magma fragments; the choked pressure, P_v, in the vent; the eruption speed, U_v, of gas and small pyroclasts; and the speeds of gas and small clasts after gas decompression to atmospheric pressure, U_{aM} and U_{aE} on Mars and Earth, respectively.

Above the vent, a series of shocks and expansion waves within the volcanic jet allows the pressure in the vent, P_v, to relax to the atmospheric pressure, P_a, over a vertical distance of at least several vent diameters. This process has been explored theoretically for expansions into a vacuum (Kieffer, 1982) or into a crater-like structure around the vent on Earth (Woods and Bower, 1995), but is not well studied for other geometries or atmospheric pressures, especially where eruptions take place into an atmosphere which must eventually begin to be entrained into the jet. Nevertheless, a reasonable approximation to the amount of energy per unit mass available from the decompression from P_v to P_a is ΔE given by

$$\Delta E = [\gamma/(\gamma-1)][(n\ Q\ T)/m]\{1 - (P_a/P_v)^{[(\gamma-1)/\gamma]}\}, \quad (5)$$

where it has been assumed that the expansion and cooling of the gas–pyroclast mixture from its eruption temperature T can be treated as the adiabatic expansion of a pseudo-gas having a ratio of specific heats γ given by

$$\gamma = (s_{sp} + \lambda\ s_r)/(s_{sv} + \lambda\ s_r) \quad (6)$$

where s_{sp} and s_{sv} are the specific heats at constant pressure and constant volume, ~3900 and ~2800 J kg^{-1} K^{-1}, respectively, of steam, s_r is the specific heat at constant volume of the silicate material, ~1000 J kg^{-1} K^{-1}, and λ is defined as

$$\lambda = (1-n)/n \quad (7)$$

The energy ΔE must be added to the kinetic energy of the eruption products at the vent level to obtain their final velocity, U_a, after reaching atmospheric pressure:

$$0.5\ U_a^2 = \Delta E + 0.5\ U_v^2. \quad (8)$$

Eqs. (1)–(4) involve only the magma water content, the magma temperature, and the physical properties of the water vapor, and so for any given magma, the values of P_f, P_v and U_v will be the same for choked eruptions on both Mars and Earth. However, the atmospheric pressure P_a is involved in calculating the final velocity via Eqs. (5)–(8), and so it is here that a significant difference appears between eruptions on Mars and Earth; we therefore give the values U_{aM} and U_{aE} for

Mars and Earth, respectively, in Table 1. We do not yet have direct information on the typical amounts and compositions of volatiles in martian magmas, though we assume that, as on Earth, H_2O commonly dominates. Evidence from SNC meteorites suggests that some samples (e.g., Shergotty) contained up to ~2% water in the magma during ascent and eruption on Mars (e.g., McSween et al., 2001). Values are given in the Table for a wide range of magma water contents, covering the amounts commonly found in oceanic basalts on Earth (e.g., Wallace and Anderson, 2000) and extending up to higher values. We note that Dixon et al. (1997) documented alkali basaltic/nephelinitic lavas erupted north of Hawaii which contained 1.9 wt.% H_2O and 5.4 wt.% CO_2; converted to an equivalent water content this would correspond to approximately [1.9+(18/44)×5.4=] 4.1 wt.% H_2O, i.e. n=~0.04, and so values up to n=0.05 are given in Table 1.

3. Behaviour of eruption products in the atmosphere

As outlined in Introduction, there are two cases to consider. In the first, we assume that models of convective plume rise developed for the Earth's atmosphere are applicable, with the appropriate changes to atmospheric properties, to plumes on Mars that rise to heights up to ~20 km. Where the traditional treatment predicts plume rise heights in excess of ~20 km, and the arguments of Glaze and Baloga (2002) imply that the treatment breaks down, we use the traditional model but truncate the plume at 20 km height. In the second case, we consider eruptions in which the plume would, if treated in the traditional way, have risen to heights greater than ~20 km. For these, we propose that the mass flux is so large that the atmosphere plays little role in controlling the dynamics, and model the upward motion of gas and pyroclasts as being dictated by inertia.

3.1. Convection plumes

The potential convective rise height of a plume is proportional to the fourth root of the heat flux injected into it, and hence essentially proportional to the fourth root of the mass flux leaving the vent. The mass flux M is given by the product of the bulk density, β, of the plume (determined in turn by the mass fraction, n, of exsolved magmatic volatiles that it contains), the cross-sectional area, C, of the plume, and the mean upward velocity, U_{aM}, of the plume contents:

$$M = \beta\ U_{aM}\ C \tag{9}$$

C and U_{aM} are the relevant values after decompression of the erupted material to atmospheric pressure. β is related to n via the volume proportions of gas and pyroclasts:

$$\beta^{-1} = (n\ Q\ T)/(m\ P_a) + [(1-n)/\rho_m] \tag{10}$$

Finally the appropriate cross-sectional area C of the plume base corresponding to a given erupted mass flux M is found from Eq. (9). We have taken a series of permutations of n and a typical value of M and used the above relationships to derive corresponding values of β and C. For easier appreciation, the values of C are converted to the radii r_v of equivalent area circular vents, i.e.

$$C = \pi\ r_v^2 \tag{11}$$

(the eruption sources may well be elongate fissures, but to give explicit dimensions we would have to adopt an aspect ratio and there is no simple theoretical way of choosing this). These parameters were then used as inputs to the model of volcanic plume rise on Mars described by Wilson and Head (1994), which is a simple modification, taking account of the structure of the martian atmosphere, of the one developed by Wilson and Walker (1987) for the Earth. The Mars atmosphere model is taken from Moudden and McConnell (2005).

To illustrate plausible eruption conditions on Mars we adopted an erupted mass flux of $M=6\times10^5$ kg s^{-1}. For a magma density of 3000 kg m^{-3} this corresponds to the typical volume flux of 200 m^3 s^{-1} observed during episodes of the well-documented basaltic lava fountain eruption at the Pu'u 'O'o vent of Kilauea volcano, Hawaii (Heliker and Mattox, 2003). Using this eruption rate, Eqs. (9)–(11) yield the eruption parameters listed in Table 2 for the same range of equivalent magma water contents used in Table 1 (the values of U_{aM} as a function of n given in Table 1 are repeated in Table 2 for completeness). Almost all of the magma volatile contents guarantee that, at this mass eruption rate, the plume will be capable of reaching ~20 km; only for the smallest volatile content shown, n=0.1%, does the model predict column instability and collapse from a low height, ~4 km, presumably to feed pyroclastic flows (Wilson and Head, 1994). The fifth column of Table 2 gives plume heights, H_{max}, that would have been expected under the assumption that the gas laws were obeyed at all heights in the martian atmosphere: they are all of order 60–70 km. However, since we now accept that plumes cannot continue to convect at heights much greater than 20 km, the sixth column of the Table gives the radii, r_p, of the plumes at this height: they lie in

Table 2
Parameters defining the properties of a convecting eruption plume on Mars for an eruption with a mass eruption rate of $M=6\times10^5$ kg s^{-1}

n (%)	U_{aM} (m s^{-1})	β (kg m^{-3})	r_v m	H_{max} km	r_p km	ϕ_p mm
0.1	95	0.897	47.4	4		
0.3	176	0.299	60.3	62	1.74	23.5
0.5	234	0.179	67.5	63	1.79	23.7
1.0	340	0.090	79.1	63	1.86	23.6
1.5	421	0.060	87.1	64	1.90	23.9
2.0	488	0.045	93.4	65	1.93	24.1
3.5	642	0.026	107.7	67	1.99	25.6
5.0	750	0.018	118.7	70	2.02	26.3

As a function of the exsolved magma water content, n (given as mass %), values are listed for the mean upward speed, U_{aM}, the bulk density of the eruption plume, β, and the radius of the plume base, r_v, after the gas component has decompressed to atmospheric pressure. Also given are the height H_{max} that the plume would have been predicted to have reached if the gas laws applied at all heights in the martian atmosphere; the radius of the plume r_p at a height of 20 km where the gas laws rapidly become inappropriate; and the diameter, ϕ_p, of the largest pyroclast with density 1500 kg m^{-3} that could be transported to a height of 20 km.

the range ~1.7–2.0 km. Finally, the conditions within the eruption plume as tracked by the model are used to define the diameter of the largest pyroclast, ϕ_p, that could be transported to a height of 20 km (a clast density of 1500 kg m^{-3} is assumed), and these, ~23–26 mm, are given in the last column of Table 2.

The nearly-constant nature of the values of r_p and ϕ_p in Table 2 (for plumes that do not become unstable and collapse from low heights) shows that conditions near the top of an eruption plume depend almost entirely on the erupted mass flux, not the details of the eruption speed and vent radius. To cover the widest possible range of eruption conditions likely on Mars, the above calculations were repeated with mass fluxes of 10^5, 10^6 and 10^7 kg s^{-1} at a constant equivalent magma water content of 2 mass %. The corresponding values of the parameters r_p and ϕ_p at 20 km height are shown in Table 3. Plume radii may approach 4 km for the very highest eruption rates, and pyroclasts with diameters up to ~35 mm could be transported to their tops.

3.2. Inertial plumes

When eruption plumes have the potential to convect to heights greater than those where the traditional assumptions about convection break down, there are again two cases to consider, now as a function of both the mass flux and the eruption speeds of the pyroclasts. If the mass flux leaving the vent is less than some critical value, entrainment of the atmosphere at low levels will still dominate the rise of the plume. The upward velocity of the plume will decrease rapidly as the volcanic materials share momentum with entrained atmospheric gas, and the velocity may rise again (but to values much less than the eruption speed) as thermal energy is converted to buoyancy. Ultimately, as the atmospheric pressure decreases and the mean free path of the molecules in the atmosphere (and in the gases in the plume) becomes large enough, the entrainment process will cease to operate, pyroclasts will decouple from the gas and begin to fall to the ground, and the plume will effectively dissipate at a much smaller height than it might have reached in a denser atmosphere. The release and dispersal of pyroclasts will be essentially the same as for the smaller mass flux plumes treated in Convection plumes.

However, if the mass flux leaving the vent is large enough, the dilution of the upward momentum of the erupted material by entrained atmosphere will be minimal, and the upward velocity will decrease much more slowly with height than in convecting plumes produced by smaller mass fluxes. At sufficiently large mass fluxes, the eruption products may be thought of as punching a hole into the atmosphere. In this case virtually all of the pyroclasts will effectively be protected from interaction with the surrounding atmosphere as they rise and will follow near-ballistic upward paths controlled only by inertia and gravity. The pyroclasts represent the bulk of the mass of the ejected volcanic material and so their motion completely dominates that of the accompanying magmatic gas. The resulting configuration will be similar to that seen in the inner parts of the eruption "plumes" on Io (Cataldo et al., 2002; Geissler, 2003; Zhang et al., 2003). In the extreme case, if the eruption speed is large enough, the clasts will rise to much greater heights than they would have reached if they had been entrained in a convecting plume. They will reach a maximum height dictated by their launch speeds and will then fall back, accelerating under gravity, into the denser, lower atmosphere from above. As they reach the ~20 km height level where the gas laws start to

Table 3
Parameters of eruption plumes for a constant magma volatile content of $n=2$ mass % and variable mass eruption rate

M kg s^{-1}	U_{aM} m s^{-1}	β kg m^{-3}	r_v m	r_p km	ϕ_p mm
10^5	477	0.045	38.6	1.51	10.4
10^6	494	0.045	119.9	2.25	28.6
10^7	505	0.045	374.9	4.01	35.3

Values are given for the mean upward speed, U_{aM}, the bulk density of the plume, β, and the radius of the plume base, r_v, after the gas component has decompressed to atmospheric pressure; and for the radius of the plume r_p at a height of 20 km where the gas laws rapidly become inappropriate and the diameter, ϕ_p, of the largest pyroclast with density 1500 kg m^{-3} that could be transported to this height.

apply, they will begin to feel the effects of drag forces and will quickly decelerate to the local terminal velocity appropriate to their sizes and densities. Their subsequent fall through the atmosphere and lateral dispersal will be determined by the atmospheric wind system in the same way as for pyroclasts released from a convecting plume, but their greater lateral travel distance while rising will mean that they are injected into the atmosphere over a wider area, i.e. at greater distances from the vent, and so are likely to experience greater dispersal.

Fig. 1 shows the geometry implied, with clasts launched at an angle θ to the vertical reaching a maximum height H at a distance X from the vent and then falling back a distance $(H-Z)$ to re-enter the denser part of the atmosphere at height Z above the surface at a radial distance $R=(X+Y)$ from the vent. If the launch speed is the eruption speed from the vent region, U_{aM}, the horizontal and vertical components of the velocity are U_{aM} sin θ and U_{aM} cos θ, respectively. The maximum rise height is found from classical ballistic theory (neglecting the curvature of the planet, justified in this case) to be $H=U_{aM}^2 \cos^2 \theta/(2\,g)$ and the distance $X=U_{aM}^2 \sin 2\theta/(2\,g)$. Finally, R is given by

$$R = X + U_{aM} \sin \theta \, [2(H-Z)/g]^{1/2} \quad (12)$$

It is difficult to predict the range of angles from the vertical at which pyroclasts will be projected upward. By analogy with the appearance of eruption plumes on Io, we assume $\theta=30°$ to be a plausible maximum angle, and we take Z as 20 km. Table 1 gives values of the eruption speeds, U_{aM}, of gas and small clasts after decompression to martian atmospheric pressure as a function of n. These are used in Table 4 to find,

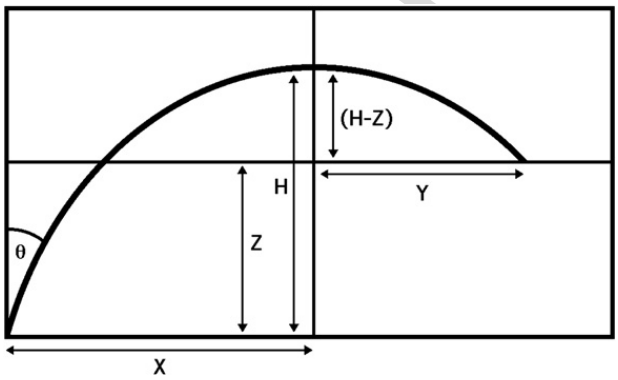

Fig. 1. Diagram showing the path of pyroclasts rising along the outer edge of an Io-type inertia-dominated eruption plume. The plume punches through the lower atmosphere and projects clasts to a height H from which they fall back into the lower atmosphere at a distance $(X+Y)$ from the vent, settling at their terminal velocities from a height $Z=\sim 20$ km.

Table 4
Parameters of inertial eruption plumes on Mars

n (%)	U_{aM} (m s^{-1})	H km	X km	Y km	R km
0.1	95	0.9	1.1		
0.3	176	3.1	3.6		
0.5	234	5.5	6.4		
1.0	340	11.7	13.5		
1.5	421	17.9	20.6		
2.0	488	24.0	27.7	11.3	39.0
3.5	642	41.5	48.0	34.6	82.5
5.0	756	57.6	66.5	53.8	120.3

For each value of the exsolved magma water content, n (given as mass %), and corresponding eruption speed from the vent, U_{aM}, values are listed for the maximum height, H, reached by pyroclasts ejected at an angle of up to $\theta=30°$ from the vertical; the lateral distance from the vent, X, at which this height is reached; the additional lateral distance, Y, travelled by pyroclasts before descending to the 20 km height in the atmosphere at which they experience significant drag forces; and the total distance from the vent, R, at which they begin to fall at their terminal velocities through the atmosphere. A blank entry means that this model is not applicable.

for each choice of n, the values of H, X, Y and R. Clearly, if clasts are required to be ejected to heights in excess of $Z=20$ km for this process to work, it will only be important for relatively volatile-rich magmas, those with an equivalent water content in excess of 1.7 wt.%.

The minimum erupted mass flux that will ensure that atmosphere entrainment in the rising part of a plume has a negligible effect on the bulk motion of the gas and pyroclasts can be found as follows. Using the basic ballistic relationships, the upward speed U_v of the gas and small clasts at the edge of the jet of material leaving the vent is given as a function of height z by

$$U_v = (U_{aM}^2 \cos^2\theta - 2\,g\,z)^{1/2} \quad (13)$$

and this speed corresponds to the edge of the jet being at a distance x from the vent where

$$x = \sin\theta[(U_{aM}^2 \cos^2\theta/g) - \{(U_{aM}^2 \cos^2\theta/g)^2 - 2\,z\,U_{aM}^2/g\}^{1/2}] \quad (14)$$

Thus the mass inflow rate M_{in} of entrained atmosphere through the edge of the jet in a horizontal slice through the jet of radius x and vertical extent dz is

$$M_{in} = 2\,\pi\,x\,\alpha\,U_v\,\rho\,dz \quad (15)$$

where ρ is the density of the atmosphere taken from Moudden and McConnell (2005) and α is the entrainment coefficient, ~0.065 (Woods, 1998). Substitution of Eqs. (13) and (14) into (15) allows the total

Table 5
Values of the minimum mass fluxes, M_{min}, required to guarantee the applicability of the inertial plume model on Mars when pyroclasts are ejected at angles of up to $\theta=10°$ and 30° from the vertical

n (%)	M_{min}, $\theta=10°$ (kg s^{-1})	M_{min}, $\theta=30°$ (kg s^{-1})	Eruption with comparable mass flux
0.1	3.0×10^4	3.6×10^4	
0.3	6.0×10^5	1.2×10^6	Pu'u 'O'o, Kilauea, Hawaii
0.5	2.2×10^6	4.8×10^6	
1.0	1.0×10^7	2.4×10^7	
1.5	2.3×10^7	5.5×10^7	Skaftár fires (Laki), Iceland
2.0	3.2×10^7	8.5×10^7	
3.5	4.6×10^7	1.3×10^8	Mt. St. Helens, U.S.A.; Tvashtar, Io
5.0	5.6×10^7	1.6×10^8	

Where well-known examples are available, eruptions on other bodies having comparable mass fluxes are indicated.

contribution to M_{in}, M_{tot}, to be evaluated numerically up to any chosen height. Despite the increase in x, the decreases with height of both U_v and ρ ensure that additional contributions to M_{tot} become very small at heights approaching 20 km. The minimum mass flux from the vent allowing the effects of the atmosphere to be ignored is then the flux M_{min} that ensures $M_{min}>M_{tot}$. Values of these minimum erupted mass fluxes are given as a function of n and the maximum angles from the vertical at which clasts are ejected, θ, in Table 5. Well-documented eruptions on Earth and Io that had similar mass fluxes to those listed are indicated; clearly there is no reason to regard the conditions required to produce inertial eruption plumes as rare.

4. Formation of accretionary lapilli on Mars

Gilbert and Lane (1994) showed that accretionary lapilli form in explosive eruption plumes on Earth when initially small particles grow by becoming coated with water condensing in the eruption plume and accreting other small particles which they overtake as they fall. The overtaken particles become trapped in the water layer, and chemical processes bond the accreting particles to one another and ensure the stability of the growing structure. The critical factors controlling the growth of a lapillus to a final size D (assumed to be much greater than its initial size) are the vertical distance through which it falls, z, and the mass loading in the eruption plume, i.e. the total mass of pyroclasts per unit volume, w. Other important factors are the density of individual ash particles, ρ_a, the porosity of the aggregates, p, the density of the liquid or gas in the pore spaces, ρ_p, and the aggregation coefficient, E, combining the efficiency of sticking and the probability of collision, which accounts for the extent to which a small particle attempts to follow streamlines in the gas and be swept around any larger clast that overtakes it. The relationship is

$$D = 0.5\ w\ E\ z/\rho_B \quad (16)$$

(Gilbert and Lane, 1994) where the lapillus bulk density ρ_B is equal to $[\rho_a - p\ (\rho_a - \rho_p)]$. Two conditions are implicit in the assumptions behind this model. The first is that large pyroclasts fall through an eruption plume faster than smaller ones. This will be true as long as the atmospheric pressure is large enough to ensure that particles interact with the gas according to the gas laws, falling with terminal velocities that are a function of their size. A comparison of the mean free paths of molecules in the martian atmosphere with the ranges of lapilli sizes considered here shows that it is only at heights greater than ~50 km on Mars that mean free paths exceed particle sizes so that the Knudsen regime becomes operative and all particles move at the same (high) speed. This is not a limitation because, as we describe below, we assume that martian eruption plumes rarely rise to heights much greater than ~20 km. More important is the fact that a liquid water film is required on the colliding clasts to aid adhesion. This is common over a wide range of heights in eruption plumes on Earth, both where clasts are rising above the vent and where they are falling at greater lateral distances. However, it is more problematic on Mars because of the low (everywhere <240 K — Moudden and McConnell, 2005) atmospheric temperatures. If a sufficient amount of atmosphere is entrained into an eruption plume on Mars, any water will be frozen to ice. However, we find that temperatures will be above the freezing point in much of the rising part of an eruption plume, and we infer that it is here that most lapilli formation occurs. The fact that the relative motion of large and small clasts is superimposed on the high-speed turbulent motion of the rising part of the eruption plume, rather than on the lower-speed, more nearly laminar motion of the atmosphere outside the rising core of the plume, as on Earth, does not hinder the formation process and, indeed, may enhance it by providing an effectively greater path length over which particle collisions can occur.

Experimental data (Gilbert and Lane, 1994) show that E in Eq. (16) is ~1 for very small adhering particles and decreases from ~1 to ~0.1 as the adhering particle size increases from ~10 to ~100 μm. ρ_a is taken as 1500 kg m^{-3} on both Earth and Mars, and is ~50%

greater than ρ_p when water fills pore spaces and is very much greater than ρ_p when gas fills them. As a compromise we assume that pore spaces are half filled with water. p is generally ~0.4 for lapilli on Earth and there is no reason to expect values to be greatly different on Mars, so that $[\rho_a - p(\rho_a - \rho_p)] = 1100$ kg m^{-3}. Well above the vent in eruption plumes on Earth, w ranges from $\sim 2\times10^{-3}$ to 10×10^{-3} kg m^{-3} (Gilbert and Lane, 1994). The major difference between explosive eruptions on Mars and Earth is that the volatiles exsolved from the magma must eventually decompress by a much greater factor to reach equilibrium with the atmosphere on Mars than on Earth. Enhanced gas expansion implies that a given mass, and hence a given number, of pyroclasts will occupy a greater volume on Mars than Earth, leading to a smaller value of w. The ratio Λ of the volatile volumes before and after adiabatic expansion is given by

$$\Lambda = [P_v/P_a]^{(1/\gamma)}. \quad (17)$$

The decompression is partly accommodated by the increase in gas velocity from U_v to U_a and partly by the increase of the cross-sectional area of the erupting jet, and it is this area change that is directly reflected by w. The factor A by which the area increases, and hence w decreases, is given by

$$A = \Lambda/(U_a/U_v) \quad (18)$$

and Table 6 gives the values A_M and A_E for Mars and the Earth, respectively. The factor by which w is smaller on Mars than Earth is equal to A_M/A_E, and since the largest value of w for terrestrial eruption plumes is $\sim 10\times10^{-3}$ kg m^{-3} (Gilbert and Lane, 1994), we divide this value by (A_M/A_E) to obtain the values of w for Mars, w_M, for each value of n in Table 6. Finally, inserting these values of w_M into Eq. (16), together with the values of the other parameters discussed earlier as being relevant to Mars, gives the values of the largest likely lapilli sizes, D, in the final column of Table 6. Values are seen to vary between ~0.7 and 0.9 mm. The smallest lapilli sizes are likely to be smaller than these values by at least a factor of 10, and we note that all of the predicted lapilli sizes are about one order of magnitude smaller than those commonly found on Earth.

Table 6
Parameters involved in the calculation of accretionary lapilli sizes on Mars

n (%)	A_M	A_E	A_M/A_E	w_M (kg m^{-3})	D (mm)
0.1	188	2.3	80.6	1.24×10^{-4}	0.90
0.3	517	5.4	96.5	1.04×10^{-4}	0.75
0.5	826	8.2	101.2	0.99×10^{-4}	0.72
1.0	1536	14.6	105.1	0.95×10^{-4}	0.69
1.5	2178	20.6	106.0	0.94×10^{-4}	0.69
2.0	2765	26.1	105.8	0.95×10^{-4}	0.69
3.5	4249	41.2	103.1	0.97×10^{-4}	0.71
5.0	5405	54.3	99.5	1.01×10^{-4}	0.73

As a function of the exsolved magma water content, n, values are given for the factor by which the area of the erupting gas–pyroclast jet expands while decompressing, A_M and A_E on Mars and Earth, respectively; the ratio of these area factors; the mass of pyroclasts per unit volume, w_M , predicted for a martian eruption plume; and the likely maximum size, D, of accretionary lapilli on Mars.

5. Grain sizes in martian pyroclastic deposits

The calculations described so far have enabled us to predict the likely maximum sizes of normal pyroclasts and of accretionary lapilli that are transported to, and released at, heights of ~20 km in the martian atmosphere, the maximum heights from which we expect them to be dispersed in the lower atmosphere. To summarize, these maximum sizes were up to ~26 mm in the case of juvenile pyroclastic particles carried convectively (Tables 2 and 3) and ~0.9 mm (Table 6) for accretionary lapilli formed from smaller particles within eruption plumes. In the case of pyroclasts injected into the upper atmosphere in the inertial mode, all sizes leaving the vent will reach the ~20 km injection height.

There remains the issue of what range of juvenile pyroclast sizes are likely to be available for transport upward in eruption plumes on Mars. Aspects of this were considered by Wilson and Head (1994) who evaluated the sizes of the largest clasts that could be transported out of the vent and into the base of an eruption plume on Mars and also discussed the role of the lower atmospheric pressure on Mars in causing a greater degree of gas release and magma fragmentation than on Earth. They found that the combinations of speed and density expected for the gas phase in explosive eruptions on Mars was such as to make it possible to transport clasts with diameters up to 200 mm out of the vent. However, applying their arguments about the effects of greater pyroclast fragmentation led to the conclusion that maximum clast sizes released in explosive eruptions on Mars were not commonly expected to be greater than a few millimeters. Thus we find that convecting eruption plumes (and inertia-dominated eruptions) have the capacity to transfer larger particles to heights of ~20 km than are likely to be initially present in the gas–particle mixture leaving the vent. Instead, the maximum sizes of particles released into the atmosphere at heights of ~20 km are

likely to be a few mm if they are juvenile clasts and ~1 mm if they have grown by accretion in a convecting plume. The smallest clasts likely to be present are defined, as on Earth, by the sizes of the smallest gas bubbles nucleating in the magma, a few tens of microns. This finding of rather uniform pyroclast size ranges independent of the formation mechanism simplifies the prediction of the dispersal of the particles as they fall to the surface.

6. Dispersal of pyroclasts

The dispersal of clasts with sizes in the tens of microns to mm range as they fall through the martian atmosphere from heights of ~20 km will depend on the wind regimes that they encounter while falling, and on their terminal velocities. Wind speeds (dominated by zonal winds) are given for the current atmosphere and northern and southern summer conditions and for low and high dust loading by Moudden and McConnell (2005), and typical conditions can be represented adequately by a wind profile that decreases roughly linearly from ~40 m s^{-1} at 20 km to zero at ground level. Clast terminal velocities depend on the density ρ and viscosity η of the atmosphere, both functions of height, and on the clast size (ϕ_p, the diameter of an equivalent sphere) and the clast density, ρ_B = ~1100 kg m^{-3} for lapilli and ρ_a = ~1500 kg m^{-3} for juvenile clasts. Using the Moudden and McConnell (2005) model we find the atmospheric pressure, temperature, density and viscosity values given in Table 7, which also shows the terminal fall velocities u_F for several sizes of particles in the 20 μm to 2 mm range for a clast density of ρ_B = 1100 kg m^{-3}. These terminal velocities are calculated for the relevant regime (laminar or turbulent) in which the particles fall by taking u_F to be the smaller of

$$u_L = (\phi_p^2\ \rho_B\ g)/(18\ \eta), \quad (19)$$

$$u_T = [(4\ \phi_p\ \rho_B\ g)/(3\ C_D\ \rho)]^{1/2}, \quad (20)$$

where g is the acceleration due to gravity, ~3.72 m s^{-2}, and C_D is a dimensionless drag coefficient that depends on the shapes of particles but is of order unity.

Using these fall speeds, incremental fall times between successive heights in the atmosphere, τ, are shown in Table 8 together with the corresponding increments, δ, of lateral displacement by the wind having speed W. The displacements depend very strongly on the clast size; mm-sized clasts can be transported only 10–20 km, and their final distribution will depend significantly on the details of the eruption that produced them. In contrast, clasts smaller than ~50 μm may commonly be transported more than 10,000 km, and during their dispersal they will lose all memory of the way they were injected into the atmosphere. Table 8 also shows the extent to which clast dispersal is dependent on the wind speed distribution in the atmosphere. Wind speeds are greatest at large heights, but here fall speeds are relatively large and clasts spend less time being influenced by the wind; wind speeds are least near the ground but here fall speeds are also small. The consequence is that it is the wind speed distribution in the middle part of the atmosphere, at heights between ~10 and ~15 km, that has the greatest influence on transport distances. Finally, note that the values in Tables 7 and 8 are calculated for a lapillus clast density of ρ_B = 1100 kg m^{-3}; if the juvenile pyroclast density of ρ_B = 1500 kg m^{-3} is used, travel distances are about 75% of those listed.

Table 7
The variation with height above the ground, H_g, of pressure, P_a, temperature, T_a, viscosity, η, density, ρ, and wind speed, W, in the martian atmosphere

H_g	P_a	T_a	η	ρ	W	u_F in m/s for clast sizes in mm equal to						
km	Pa	K	10^{-6} Pa s	kg/m^3	m/s	2	1	0.5	0.2	0.1	0.05	0.02
20.0	104	185	10.0	0.0030	40	74.1	26.9	6.72	1.07	0.269	0.0672	0.0107
19.0	115	187	10.1	0.0033	38	70.9	26.7	6.68	1.07	0.267	0.0668	0.0107
17.0	139	188	10.1	0.0039	34	64.8	26.6	6.65	1.06	0.266	0.0665	0.0106
15.0	168	190	10.2	0.0047	30	59.1	26.5	6.62	1.06	0.265	0.0662	0.0106
12.5	213	191	10.2	0.0059	25	52.7	26.3	6.58	1.05	0.263	0.0658	0.0105
10.0	270	192	10.3	0.0074	20	46.9	26.1	6.52	1.04	0.261	0.0652	0.0104
7.5	343	196	10.4	0.0093	15	42.1	25.8	6.46	1.03	0.258	0.0646	0.0103
5.0	435	200	10.5	0.0115	10	37.7	25.6	6.40	1.02	0.256	0.0640	0.0102
2.5	552	208	10.9	0.0140	5	34.1	24.1	6.16	0.99	0.246	0.0616	0.0099
0.0	700	220	11.5	0.0168	0	31.2	22.0	5.84	0.93	0.234	0.0584	0.0093

The terminal velocities, u_F, of lapilli with the sizes indicated and a density of 1100 kg m^{-3} are given at each height.

Table 8
Parameters needed in the calculation of the lateral displacement by the wind of clasts falling through the atmosphere

	fall times τ and displacements δ for clast diameters in mm equal to													
	2		1		0.5		0.2		0.1		0.05		0.02	
Hg km	τ s	δ km	τ s	δ km	τ s	δ km	τ s	δ km	τ s	δ km	τ s	δ km	τ s	δ km
20.0														
	14	0.5	44	1.7	176	6.9	1102	43	4410	172	17639	688	110245	4300
19.0														
	29	1.1	89	3.3	355	13.1	2216	82	8864	328	35454	1312	221590	8199
17.0														
	32	1.1	89	3.1	356	12.5	2227	78	8908	312	35630	1247	222689	7794
15.0														
	45	1.5	112	3.7	448	14.8	2797	92	11189	369	44758	1477	279736	9231
12.5														
	50	1.6	113	3.5	451	14.0	2818	87	11272	349	45087	1398	281793	8736
10.0														
	56	1.5	114	3.1	455	12.5	2845	78	11382	313	45527	1252	284542	7825
7.5														
	63	1.4	115	2.6	460	10.3	2873	65	11492	259	45967	1034	287292	6464
5.0														
	70	1.0	118	1.8	471	7.1	2941	44	11763	176	47051	706	294069	4411
2.5														
	77	0.4	123	0.6	492	2.5	3077	15	12308	62	49232	246	307697	1538
0.0														
		10.2		23.4		93.6		585		2,340		9,360		58,498

For each change in height H_g from a given row to the row below, the fall time τ at the terminal velocity given in Table 7 is shown, together with the lateral displacement δ caused during this time by the average wind speed (derived from the wind speeds in Table 7) relevant to the height interval. At the foot of the table the displacement increments are summed to give the total lateral distance in km that a clast of a given size travels while falling.

Using a standard Earth atmosphere temperature and density model but the same wind speed profile and 20 km eruption plume height as used for Mars, the equivalent transport distances on Earth for large (a few mm in size) clasts are found to be roughly a factor of four greater than on Mars. However, small (less than ~0.2 mm in size) clasts travel further on Mars than on Earth by a factor of about two. The differences are complex functions of the differing values of the acceleration due to gravity, and of the differing atmospheric composition, pressure and temperature, and hence density and viscosity. For a realistic terrestrial wind speed profile, with the speed reaching a maximum of ~20 m s^{-1} at ~13 km elevation and decreasing to ~10 m s^{-1} at 20 km height (Valley, 1965), the transport distances on Earth would be about 40% of those produced by the Mars wind profile.

Finally, we consider the possibility that conditions on Mars were different in the early part of its geologic history, with the atmospheric pressure, and hence temperature, being higher than at present. Indeed, some models of early Mars assert that the atmospheric pressure may have been at least as high as that on Earth now (Fanale et al., 1992), leading to as much as a four-fold reduction in plume height for a given mass eruption rate (Wilson and Head, 1994). However, a higher atmospheric pressure on Mars would mean that the atmosphere entrainment assumptions commonly made in modeling would be more completely justified, and so eruption plumes from high mass flux eruptions would have been stable to heights very much greater than the ~20 km limit applicable today, perhaps ~50 km. A higher atmospheric pressure would probably mean that regional pressure gradients, and hence typical wind-speeds, would be somewhat smaller than at present. These factors combine to suggest that eruptions on early Mars may have led to greater dispersal distances than under current conditions, by a factor of perhaps two. Some of these issues are discussed in more detail by Hort and Weitz (2001).

7. Summary of tephra and lapilli characteristics

A large number of studies have interpreted Noachian and Hesperian blanketing deposits and edifices to have involved explosive pyroclastic eruptions, and a significant number of these are interpreted to have involved groundwater and/or magmatic water (e.g., Carr, 1973;

Greeley and Spudis, 1981; Mouginis-Mark et al., 1982; Greeley and Crown, 1990; Grant and Schultz, 1990; Moore, 1990; Crown and Greeley, 1993; Robinson et al., 1993; Wilson and Head, 1994; Greeley et al., 2000; Tanaka, 2000; Hort and Weitz, 2001; Glaze and Baloga, 2002; Hynek et al., 2003; Fassett and Head, in press). Lacking, however, is definitive evidence for such origins at the regional scale, due primarily to the broad blanketing nature of the regional deposits, potential blanketing of source vents, the small grain size of the particles, and the lack of distinctive associated morphologic features (such as the long linear flows and sinuous flow fronts typical of effusive eruptions). The advent of surface exploration (e.g., landers, rovers) has increased the potential for examining deposits of such origin in much more detail. We now summarize how juvenile and accretionary clast sizes may differ between Mars and Earth, describe criteria for the recognition of these deposits at the outcrop scale on Mars, and explore some deposits at the Mars Exploration Rover Gusev and Meridiani landing sites as candidates for tephra and accretionary lapilli.

Juvenile pyroclasts produced in explosive eruptions driven by magmatic volatiles on Earth have a very wide range of sizes, from the smallest particles created from the inter-connection of freshly-nucleated gas bubbles a few tens of microns in size up to meters. Clast sizes produced in hydrovolcanic explosions are controlled mainly by the dynamics of the magma-groundwater interactions and are commonly concentrated between 0.1 and 3 mm, although some very coarse and very fine particles are also produced (Wohletz, 1983). One aspect of the low atmospheric pressure on Mars is to limit the size of the largest clast that can be transported out of a vent by expanding magmatic gases to a value of ~0.2 m. However, the enhancement of volatile exsolution and gas bubble expansion caused by the low martian atmospheric pressure should lead to more thorough magma fragmentation on Mars, so that the largest clast size commonly produced may be only a few mm in size. Thus both magmatic and hydrovolcanic explosive eruptions tend to produce similar clast size distributions on Mars. A consequence of the small juvenile pyroclast sizes is that heat exchange between erupted clasts and associated atmospheric gas, whether in the lower parts of sustained martian eruption plumes or during the flight of pyroclasts from transient hydrovolcanic explosions, will be more efficient than on Earth. Thus it is not likely that clasts falling to the ground near the vent will be hot enough to weld, as sometimes happens in plinian eruptions on Earth (Sparks et al., 1981). The relative amounts of sorting during ascent within an eruption plume and subsequent descent through the atmosphere from the plume to the ground will be similar on Mars and Earth, the only major difference being the smaller absolute grain sizes on Mars.

The generally smaller grain sizes of pyroclasts produced in martian eruptions mean that more small particles should be present to act as nuclei for condensation of water vapor in a convecting eruption plume as on Earth. Thus we expect that all pyroclasts, not just accretionary lapilli, will efficiently scavenge water from eruption plumes on Mars. The water will be in the form of ice by the time clasts reach the ground and so pyroclastic deposits may commonly have contained up to a few weight percent ice, mostly derived from the magmatic water content. The vapor pressure of the ice will have been low, but over sufficiently long periods of time chemical reactions between subliming vapor and solids may have led to some induration of the deposits.

Accretionary lapilli observed on Earth are rounded balls of tephra between 2 and 64 mm diameter consisting of smaller ash grains accreted together in an eruption plume in a process involving moisture and electrostatic forces. They commonly form in tephra sequences in beds of variable thickness consisting of poorly sorted (with wide variations in grain size) to well-sorted lapilli. The distinctive accretionary process results in anomalously large tephra particle sizes and thus accretionary lapilli tend to settle out of the eruption column closer to the vent than other tephra particles, often resulting on Earth in anomalous near-vent thickening of the deposit (e.g., Veitch and Woods, 2001). As we described above, accretionary lapilli on Mars will be characterized by sizes, ~0.1–1 mm, that are typically about one and a half orders of magnitude smaller than those on Earth; the thinner martian atmosphere tends to favor deposition near the vent, but under some circumstances the very small accretionary lapilli may be dispersed more widely than typical accretionary lapilli on Earth. In summary, on the basis of our analysis, we would anticipate accretionary lapilli deposits on Mars to have particles in the ~0.1–1 mm range, with decreasing bed thickness and grain size, and increased sorting, with increased distance from the vent and eruption column site.

8. Discussion and conclusions

On the basis of the characteristics and dispersal patterns described above, we now assess the types of observations that might lead to the recognition of tephra deposits in the geological record of Mars from different

exploration platforms. First, from an orbital perspective, data from thermal emission, VIS/NIR reflectance spectrometer, gamma ray/neutron spectrometer, and imaging instruments could detect aspects of these deposits. For example, tephra deposits should be characterized by very fine grain sizes, co-deposited water either as snow/ice or hydrated minerals, candidate low-temperature alteration products from co-deposited water, draping and mantling stratigraphic relationships, and pitting and eolian modification from the desiccation of potentially ice-containing tephra deposits and their subsequent dispersal.

Lander and rover platforms provide a more detailed perspective. The Mars Exploration Rover (MER) Spirit has been exploring the floor of Gusev Crater for several years and has found the crater floor to be covered with basaltic lavas of probable Hesperian age (Squyres et al., 2004a) underlying a thin impact-generated and reworked regolith. The Hesperian-aged volcanic edifice Apollinaris Patera (thought to have been the site of water-rich pyroclastic eruptions, e.g., Robinson et al. (1993)) lies ~280 km north of the Gusev crater rim (Fig. 2). Thus, on the basis of our analysis of ash and lapilli, there is a high likelihood that the interior of Gusev was once the location of tephra deposition.

Once leaving the olivine basalt volcanic plains and ascending into the Columbia Hills, rising ~90 m above the plain, Spirit began to encounter a diversity of pre-plains rock types, including layered deposits with variable bed thickness and grain sizes, and evidence

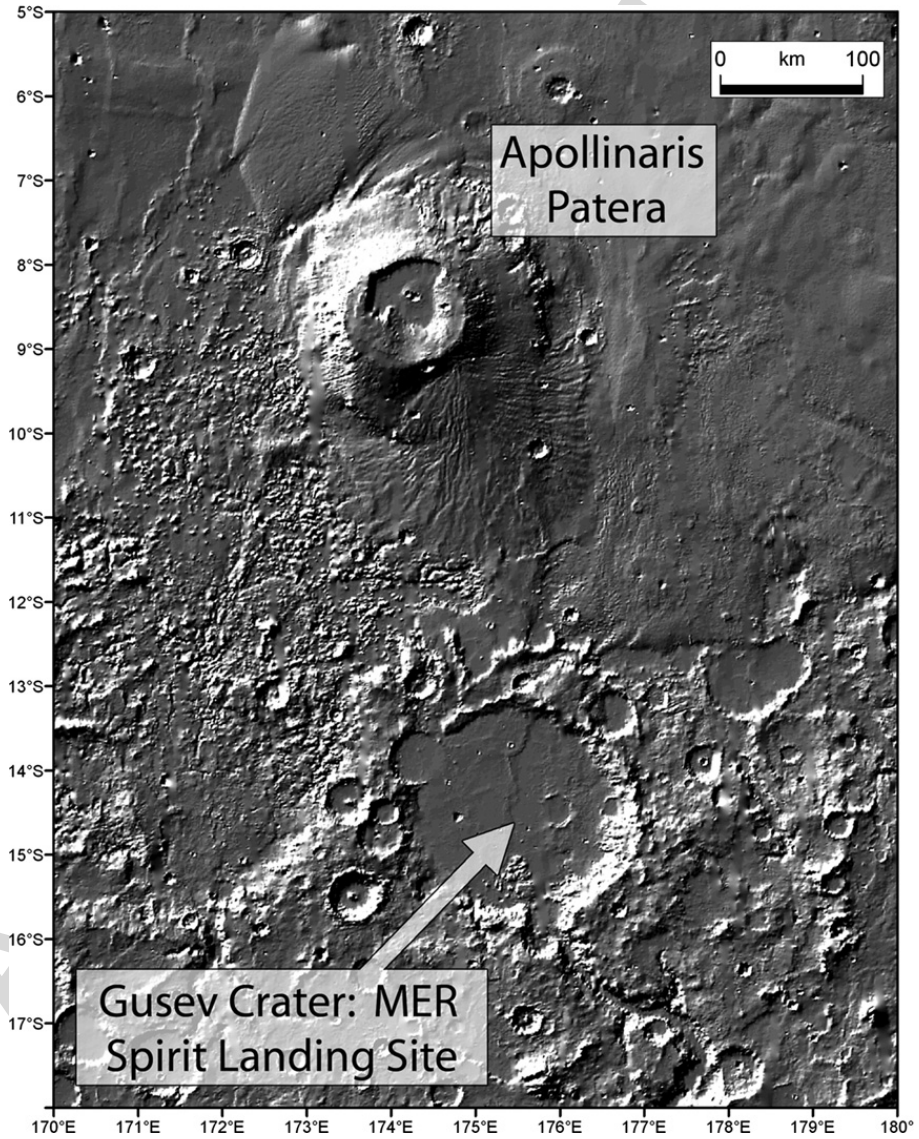

Fig. 2. Apollinaris Patera, a volcanic construct just north of Gusev Crater, the landing site for the Mars Exploration Rover *Spirit*. Eruptions from Apollinaris Patera could have been the source for pyroclastic deposits discovered by the Spirit rover (e.g., Squyres et al., 2006) on the flanks of the Columbia Hills inside Gusev Crater about 350 km to the south of the volcano. Base map is MOLA shaded relief.

(including "bomb sags") for possible pyroclastic eruptions (Squyres et al., 2006; Farrand et al., 2006; Arvidson et al., 2006; Herkenhoff et al., 2006). Some of the Columbia Hills rocks were much softer than the olivine basalts of the plains, were highly variable in surface texture and composition, and could be subdivided into five distinct classes. Among these, Clovis-class rocks range in outcrop bedding from finely laminated to massive, and contain clasts that range in size up to several mm, with some more resistant clasts differentially eroding out onto stalks; emplacement by explosive volcanism is one candidate interpretation for this class. Wishstone-class rocks contain poorly-sorted, angular, sometimes shard-like clasts in a fine-grained matrix, with textures that have been compared to those of ash-flow tuffs; explosive volcanic eruptions are considered a likely possible origin (Squyres et al., 2006). Peace-class rocks are finely layered and granular, with individual clasts up to a few mm in size, and weather to a porous, spongy texture. Composed of ultramafic sand cemented by sulfates, this class is interpreted to be sedimentary (Squyres et al., 2006).

McSween et al. (2006) recently reported evidence of an alkaline volcanic rock suite from the Columbia Hills in Gusev Crater. Three classes of fine-grained or fragmental, relatively unaltered rocks found there (Irvine, Backstay and Wishstone classes) are interpreted to be mildly alkaline basalt, trachybasalt, and tephrite, respectively. Indeed, Wishstone-class rocks have textures (surfaces decorated with closely spaced knobs and pits, with the knobs interpreted to represent small clasts; microscopic images showing angular clasts and grains of varying sizes resembling pyroclastic tuffs; Farrand et al., 2006; Squyres et al., 2006) that are consistent with a pyroclastic origin. On the basis of our analysis we conclude that within Gusev Crater the Columbia Hills are candidate sites for the location of explosive volcanic eruptions and accretionary lapilli.

Subsequent MER Gusev Crater exploration has traversed the inner basin of the Columbia Hills, an amphitheater-shaped lowland that opens to the west toward the basaltic plains (e.g., Arvidson et al., 2007). During this phase, the details of Home Plate, an ~90 m diameter approximately circular-shaped low plateau about 2–4 m high have been described (Cabrol, 2006; Rice et al., 2006; Schmidt et al., 2006; Aharonson et al., 2006; Ruff, 2006; Herkenhoff et al., 2007; Ennis et al., 2007). Home Plate is composed of inward-dipping layered rock (5–20°; Aharonson et al., 2006). Cabrol (2006) described Barnhill and Rogen, two outcrops at the margins of Home Plate: Barnhill contains ash-sized particles, and granule-sized particles, interpreted as possible lapilli; Rogan consists of granular, layered, commonly cross-bedded rocks. Rice et al. (2006) define two major subunits: the lower unit is fairly coarse-grained (sub-rounded to rounded coarse granules up to several mm in diameter), massive, poorly sorted, with wavy undulations. Rice et al. (2006) interpreted the sub-rounded to rounded coarse granules to be accretionary lapilli. A bomb sag is also seen in the lower unit. The upper unit is a finer-grained, finely laminated, moderately sorted, matrix-supported, cross-bedded clastic rock. The two units are capped with blocks of scoriaceous basaltic rock. These two units have been interpreted to have formed by hydrovolcanic explosions, building a tuff ring or maar, which has been eroded subsequently (e.g., Rice et al., 2006; Schmidt et al., 2006; Ennis et al., 2007). The bedding, and the grain size of the ash and granular deposits, are all consistent with the products of pyroclastic eruptions, but it is the size of the bomb in the bomb sag (~40 mm, a factor of 2–3 larger than what is expected for juvenile clasts produced in magmatic explosive events) that suggests the likelihood of a hydrovolcanic source. The terminal velocity of a clast of this size, ~160 m s^{-1} from Eq. (20), implies a maximum wind-transport distance of only a few km, irrespective of the source of the clast. A much greater range would be reached if the clast were ejected at a large angle from the vertical in a transient hydrovolcanic explosion, but even then the likely maximum distance to which such a clast could be thrown on Mars is much less than 100 km (Fagents and Wilson, 1996). Taken together these facts strongly suggest that, in the case of Home Plate, there were local sources (within Gusev) for at least some of the activity.

Prior to the landing at the Meridiani MER site, there were two hypotheses for the regional deposits. In one, the regional deposits were considered to be of possible pyroclastic origin (Hynek et al., 2002; Arvidson et al., 2003), whereas in the other, they were considered to be lake deposits (Christensen and Ruff, 2004). Detailed exploration of the surface rocks at the site itself revealed significant evidence supporting an interpretation involving deposition and modification in an aqueous sedimentary environment (e.g., Squyres et al., 2004b; Grotzinger et al., 2005). In an alternative interpretation, McCollom and Hynek (2005) hypothesize that the history of the Meridiani bedrock can be explained as beginning with deposition of volcanic tephra, followed by reaction with condensed fumarolic sulfur dioxide and water-bearing vapor. Our analysis may help to provide criteria to distinguish between these hypotheses.

Explosive volcanic eruptions are likely to have been common throughout the history of Mars. Wide dispersal

and thick deposits of tephra resulting from these eruptions are predicted from eruption plume heights and atmospheric circulation patterns and the convecting explosive eruption plumes are likely to have contained large amounts of water. Water ice is likely to have been a non-trivial component of the tephra deposits. In the Mars environment, accretionary lapilli can be produced from condensation of water on small particles and the consequent accretion of other particles as the smaller particles travel through the plume. The spatial distribution and grain sizes of accretionary lapilli pyroclastic fall deposits differ significantly from those involving discrete clasts with negligible clast interactions.

We have produced an improved model of the eruption and dispersal of tephra and the formation of accretionary lapilli on Mars and predicted the geometry and grain size of deposits formed from explosive eruption plumes. The properties of deposits interpreted to be of volcaniclastic origin described in the Columbia Hills region of the Mars Exploration Rover Gusev site are consistent with local explosive eruptions and also with eruptions originating from nearby Apollinaris Patera. These predictions and descriptions will be helpful in the interpretation of rocks and soils seen in future surface exploration of Mars. Combination of this basic model and atmospheric general circulation models will assist in the understanding of regional and global tephra dispersal patterns and the resulting deposits from specific vent locations. In summary, the analysis outlined here will provide data that will aid in the interpretation of explosive pyroclastic eruption products from orbit, at the MER sites, and at other upcoming lander exploration sites.

Acknowledgments

Financial assistance to JWH from the NASA Planetary Geology and Geophysics Program, and to LW from PPARC Grant PPA/G/S/2000/00521, is greatly appreciated. Thanks are extended to Caleb Fassett for productive discussions, to Mikhail Kreslavsky, Laura Kerber and Michael Wyatt for comments on the manuscript, to Steve Baloga and an unidentified reviewer for helpful comments, and to Anne Côté for help in manuscript preparation.

References

Aharonson, O., et al., 2006. Structure and stratigraphy of Home Plate from the Spirit Mars Exploration Rover. Eos, Trans. – Am. Geophys. Union 87 (52) (Fall Meet. Suppl., Abstract P44A-05).

Arvidson, R.E., et al., 2003. Mantled and exhumed terrains in Terra Meridiani, Mars. J. Geophys. Res. 108. doi:10.1029/2002JE001982.

Arvidson, R.E., et al., 2006. Overview of the Spirit Mars Exploration Rover mission to Gusev Crater: landing site to Backstay Rock in the Columbia Hills. J. Geophys. Res. 111. doi:10.1029/2005JE002499.

Arvidson, R.E., et al., 2007. Spirit's winter campaign in the inner basin, Columbia Hills, Gusev Crater. Lunar Planet. Sci. 38 (Abstract 1122).

Cabrol, N.A., 2006. Sedimentology of Home Plate at Gusev Crater, Mars. Eos, Trans. – Am. Geophys. Union 87 (52) (Fall Meet. Suppl., Abstract P44A-06).

Carr, M.H., 1973. Volcanism on Mars. J. Geophys. Res. 78, 4049–4062.

Cataldo, E., Wilson, L., Lane, S., Gilbert, J., 2002. A model for large-scale volcanic plumes on Io: implications for eruption rates and interactions between magmas and near-surface volatiles. J. Geophys. Res. 107 (E11), 5109. doi:10.1029/2001JE001513.

Christensen, P.R., Ruff, S.W., 2004. Formation of the hematite-bearing unit in Meridiani Planum: evidence for deposition in standing water. J. Geophys. Res. 109 (E08003). doi:10.1029/2003JE002233.

Cook, A.F., Shoemaker, E.M., Smith, B.A., 1979. Dynamics of volcanic plumes on Io. Nature 280, 743–746.

Crown, D.A., Greeley, R., 1993. Volcanic geology of Hadriaca Patera and the eastern Hellas region of Mars. J. Geophys. Res. 98, 3431–3451.

Dixon, J.E., Clague, D.A., Wallace, P., Poreda, R., 1997. Volatiles in alkalic basalts from the North Arch volcanic field, Hawaii: extensive degassing of deep submarine-erupted alkalic series lavas. J. Petrol. 38, 911–939.

Ennis, M.E., et al., 2007. Hydorvolcano on Mars: a comparison of Home Plate a, Gusev Crater and Zuni Salt Lake maar, New Mexico. Lunar Planet. Sci. 38 (Abstract 1966).

Fagents, S.A., Wilson, L., 1996. Numerical modelling of ejecta dispersal from transient volcanic explosions on Mars. Icarus 123, 284–295.

Fanale, F.P., Postawko, S.E., Pollack, J.B., Carr, M.H., Pepin, R.O., 1992. Mars: Epochal climate change and volatile history. In: Kieffer, H., et al. (Ed.), Mars. Univ. Arizona Press, Tucson, pp. 1135–1179.

Farrand, W.H., Bell III, J.F., Johnson, J.R., Squyres, S.W., Soderblom, J., Ming, D.W., 2006. Spectral variability among rocks in visible and near-infrared multispectral Pancam data collected at Gusev crater: examinations using spectral mixing analysis and related techniques. J. Geophys. Res. 111 (E02S15). doi:10.1029/2005JE002495.

Fassett, C.I., Head, J.W., in press. Layered mantling deposits in Northeast Arabia Terra, Mars: Noachian-Hesperian sedimentation, erosion, and terrain inversion. J. Geophys. Res.

Geissler, P.E., 2003. Volcanic activity on Io during the Galileo era. Annu. Rev. Earth Planet. Sci. 31, 175–211.

Gilbert, J.S., Lane, S.J., 1994. The origin of accretionary lapilli. Bull. Volcanol. 56, 398–411.

Glaze, L.S., Baloga, S.M., 2000. Stochastic-ballistic eruption plumes on Io. J. Geophys. Res. 105 (E7), 17579–17588.

Glaze, Baloga, S.M., 2002. Volcanic plume heights on Mars: limits of validity for convective models. J. Geophys. Res. 107 (E10). doi:10.1029/2001JE001830.

Grant, J.A., Schultz, P.H., 1990. Gradational epochs on Mars — evidence from west-northwest of Isidis Basin and Electris. Icarus 84, 166–195.

Greeley, R., Spudis, P.D., 1981. Volcanism on Mars. Rev. Geophys. Space Phys. 19, 13–41.

Greeley, R., Crown, D.A., 1990. Volcanic geology of Tyrrhena Patera, Mars. J. Geophys. Res. 95, 7133–7149.

Greeley, R., et al., 2000. Volcanism on the Red Planet: Mars. In: Zimbelman, J.R., Gregg, T.K.P. (Eds.), Environmental Effects on

Volcanic Eruptions: From Deep Oceans to Deep Space. Kluwer, New York, NY, pp. 75–112.
Grotzinger, J.P., et al., 2005. Stratigraphy and sedimentology of a dry to wet eolian depositional system, Burns formation, Meridiani Planum, Mars. Earth Planet. Sci. Lett. 240, 11–72.
Heliker, C., Mattox, T.N., 2003. The first two decades of the Pu'u 'O'o-Kupaianaha eruption: chronology and selected bibliography. In: Heliker, C., et al. (Ed.), The Pu'u 'O'o-Kupaianaha eruption of Kilauea volcano, Hawaii: the first 20 years. . U. S. Geol. Survey Prof. Paper 1676. U.S. Geol. Survey, Washington, DC, pp. 1–28.
Herkenhoff, K.E., et al., 2006. Overview of the microscopic imager investigation during Spirit's first 450 sols in Gusev crater. J. Geophys. Res. 111. doi:10.1029/2005JE002574.
Herkenhoff, K.E., et al., 2007. Overview of recent Athena microscopic imager results. Lunar Planet. Sci. 38 (Abstract 1421).
Hort, M., Weitz, C.M., 2001. Theoretical modeling of eruption plumes on Mars under current and past climates. J. Geophys. Res. 106 (E9), 20,547–20,562.
Hynek, B.M., Arvidson, R.E., Phillips, R.J., 2002. Geologic setting and origin of Terra Meridiani hematite deposit on Mars. J. Geophys. Res. 107. doi:10.1029/2002JE001891.
Hynek, B.M., Phillips, R.J., Arvidson, R.E., 2003. Explosive volcanism in the Tharsis region: global evidence in the Martian geologic record. J. Geophys. Res. 108. doi:10.1029/2003JE002062.
Kieffer, S.W., 1982. Factors governing the structure of volcanic jets. In: Boyd, F.R. (Ed.), Explosive Volcanism: Inception, Evolution and Natural Hazards. Nat. Acad. Sci. Press, Washington, D.C., pp. 143–157.
Kieffer, S.W., 1995. Numerical models of caldera-scale volcanic eruptions on Earth, Venus, and Mars. Science 269 (5229), 1385–1391.
Kusanagi, M., Matsui, M., 1998. The change of eruption styles of martian volcanoes and estimates of the water content of the martian mantle. Phys. Earth Planet. Inter. 117, 437–447.
McCollom, T.M., Hynek, B.M., 2005. A volcanic environment for bedrock diagenesis at Meridiani Planum on Mars. Nature 438, 1129–1131.
McSween, H.Y., Grove, T.L., Lentz, R.C.F., Dann, J.C., Holzheid, A.H., Riciputi, L.R., Ryan, J.G., 2001. Geochemical evidence for magmatic water within Mars from pyroxenes in the Shergotty meteorite. Nature 409, 487–490.
McSween, H.Y., Ruff, S.W., Morris, R.V., Bell III, J.F., Herkenhoff, K., Gellert, R., Stockstill, K.R., Tornabene, L.L., Squyres, S.W., Crisp, J.A., Christensen, P.R., McCoy, T.J., Mittlefehldt, D.W., Schmidt, M., 2006. Alkaline volcanic rocks from the Columbia Hills, Gusev crater, Mars. J. Geophys. Res. 111 (E09S91). doi:10.1029/2006JE002698.
Mitchell, K.L., 2005. Coupled conduit flow and shape in explosive volcanic eruptions. J. Volcanol. Geotherm. Res. 143, 187–203.
Moore, J.M., 1990. Nature of the mantling deposit in the heavily cratered terrain of northeastern Arabia, Mars. J. Geophys. Res. 95, 14,279–14,289.
Moudden, Y., McConnell, J.C., 2005. A new model for multiscale modeling of the Martian atmosphere, GM3. J. Geophys. Res. 110. doi:10.1029/2004JE002354.
Mouginis-Mark, P.J., Head III, J.W., Wilson, L., 1982. Explosive volcanism on Hecates Tholus, Mars — investigation of eruption conditions. J. Geophys. Res. 87, 9890–9904.
Mouginis-Mark, P.J., Wilson, L., Zimbelman, J.R., 1988. Polygenic eruptions on Alba Patera, Mars. Bull. Volcanol. 50, 361–379.
Rice, J.W., et al., 2006. Origin of Home Plate, Columbia Hills, Mars: hydrovolcanic hypothesis. Eos, Trans. – Am. Geophys. Union 87 (52) (Fall Meet. Suppl., Abstract P41B-1274).
Robinson, M.S., et al., 1993. Chronology, eruption duration, and atmospheric contribution of the Martian volcano Apollinaris Patera. Icarus 104, 301–323.
Ruff, S.W., 2006. Spirit's Home Run: more mineralogical diversity as observed by Mini-TES on the traverse to and arrival at Home Plate in the Columbia Hills of Gusev Crater, Mars. Eos, Trans. – Am. Geophys. Union 87 (52) (Fall Meet. Suppl., Abstract P44A-04).
Schmidt, M.E., et al., 2006. Geochemical evidence for the volcanic origin of Home Plate in the inner basin of the Columbia Hills, Gusev Crater. Eos, Trans. – Am. Geophys. Union 87 (52) (Fall Meet. Suppl., Abstract P44A-07).
Sparks, R.S.J., Wilson, L., Sigurdsson, H., 1981. The pyroclastic deposits of the 1875 eruption of Askja, Iceland. Philos. Trans. R. Soc. Lond., A 299, 242–273.
Squyres, S.W., et al., 2004a. The Spirit Rover's Athena Science Investigation at Gusev Crater, Mars. Science 305, 794–800.
Squyres, S.W., et al., 2004b. In situ evidence for an ancient aqueous environment at Meridiani Planum, Mars. Science 306, 1709–1714.
Squyres, S.W., et al., 2006. Rocks of the Columbia Hills. J. Geophys. Res. 111 (E02S11). doi:10.1029/2005JE002562.
Tanaka, K.L., 2000. Dust and ice deposition in the martian geologic record. Icarus 144, 254–266.
Tanaka, K.L., Scott, D.H., Greeley, R., 1992. Global stratigraphy. In: Kieffer, H.H., et al. (Ed.), Mars. Univ. Arizona Press, Tucson, AZ, pp. 345–382.
Valley, S.L., 1965. Chapter 4 in Handbook of Geophysics and Space Environments. McGraw-Hill, New York.
Veitch, G., Woods, A.W., 2001. Particle aggregation in volcanic eruption columns. J. Geophys. Res. 106, 26,425–26,442.
Wallace, P., Anderson, A.T., 2000. Volatiles in magmas. In: Sigurdsson, H. (Ed.), Encyclopedia of Volcanoes. Academic Press, San Diego, pp. 149–170 (Ed. in Chief).
Wilson, L., 1980. Relationships between pressure, volatile content and ejecta velocity in three types of volcanic explosion. J. Volcanol. Geotherm. Res. 8, 297–313.
Wilson, L., Head, J.W., 1981. Ascent and eruption of basaltic magma on the Earth and Moon. J. Geophys. Res. 86, 2971–3001.
Wilson, L., Walker, G.P.L., 1987. Explosive volcanic eruptions, VI. Ejecta dispersal in plinian eruptions: the control of eruption conditions and atmospheric properties. Geophys. J. R. Astron. Soc. 89, 657–679.
Wilson, L., Head III, J.W., 1994. Mars: review and analysis of volcanic eruption theory and relationships to observed landforms. J. Geophys. Res. 32, 221–263.
Wohletz, K.H., 1983. Mechanisms of hydrovolcanic pyroclast formation: grain-size, scanning electron microscopy, and experimental studies. J. Volcanol. Geotherm. Res. 17, 31–63.
Woods, A.W., 1998. Observations and models of volcanic eruption columns. In: Gilbert, J.S., Sparks, R.S.J. (Eds.), The Physics of Explosive Volcanic Eruptions. Geol. Soc. Lond. Spec. Publ., vol. 145, pp. 91–114.
Woods, A.W., Bower, S.M., 1995. The decompression of volcanic jets in a crater during explosive volcanic eruptions. Earth Planet. Sci. Lett. 131 (3–4), 189–205.
Zhang, J., Goldstein, D.B., Varghese, P.L., et al., 2003. Simulation of gas dynamics and radiation in volcanic plumes on Io. Icarus 163, 182–197.